

Force-Dependent Stepping Kinetics of Myosin-V

Anabel E.-M. Clemen,* Mojca Vilfan,[†] Johann Jaud,* Junshan Zhang,* Michael Bärmann,* and Matthias Rief*

*Physics Department E22, Technical University Munich, 85747 Garching, Germany; and [†]J. Stefan Institute, 1000 Ljubljana, Slovenia

ABSTRACT Myosin-V is a processive two-headed actin-based motor protein involved in many intracellular transport processes. A key question for understanding myosin-V function and the communication between its two heads is its behavior under load. Since *in vivo* myosin-V colocalizes with other much stronger motors like kinesins, its behavior under superstall forces is especially relevant. We used optical tweezers with a long-range force feedback to study myosin-V motion under controlled external forward and backward loads over its full run length. We find the mean step size remains constant at ~36 nm over a wide range of forces from 5 pN forward to 1.5 pN backward load. We also find two force-dependent transitions in the chemomechanical cycle. The slower ADP-release is rate limiting at low loads and depends only weakly on force. The faster rate depends more strongly on force. The stronger force dependence suggests this rate represents the diffusive search of the leading head for its binding site. In contrast to kinesin motors, myosin-V's run length is essentially independent of force between 5 pN of forward to 1.5 pN of backward load. At superstall forces of 5 pN, we observe continuous backward stepping of myosin-V, indicating that a force-driven reversal of the power stroke is possible.

INTRODUCTION

Myosin-V is a molecular motor involved in intracellular organelle and vesicle transport (Reck-Peterson et al., 2000). It converts chemical energy into work through a cycle which involves nucleotide hydrolysis. Unlike conventional myosin-II, myosin-V is a processive motor that moves in 36 nm steps along the actin filaments (Mehta et al., 1999). Processivity combined with a large step size makes this motor ideal for studying chemomechanical energy conversion at the single-molecule level. Bulk as well as single-molecule kinetic studies have shown that ADP release is the rate-limiting transition in the myosin-V chemomechanical cycle (De La Cruz et al., 1999; Rief et al., 2000; Wang et al., 2000). Single-molecule studies comparing double headed myosin-V with single headed myosin-V constructs (Purcell et al., 2002; Veigel et al., 2002) suggest that the large step size of 36 nm is a combination of a power stroke and a diffusive motion. The putative power stroke has indirectly been observed by single-molecule fluorescence polarization studies when a large angular change of the neck domain of myosin-V during one step has been visualized (Forkey et al., 2003). Recently, Yildiz et al. (2003) provided direct evidence for a hand-over-hand mechanism for myosin-V motility in single-molecule fluorescence studies.

The motion of molecular motors is affected by mechanical loads. Studying the stepping kinetics as a function of mechanical load can thus provide detailed insights into the force-dependent rates in the chemomechanical cycle. This has already been achieved for other linear motors, like kinesin (Visscher et al., 1999) and myosin-VI (Altman et al., 2004). Although the force dependence of the average speed of myosin-V has been measured (Mehta et al., 1999; Uemura

et al., 2004), an identification of the load-dependent transitions is still missing. This is especially important since models for myosin-V motility call for a strong load dependence of ADP release for the communication between the two heads (Veigel et al., 2002). Moreover, in its physiological environment, myosin-V colocalizes with other motors like kinesin in melanosome transport (Huang et al., 1999; Mermall et al., 1998). Situations where myosin-V is involved in a tug-of-war with a much stronger kinesin motor with stall forces in the 5 pN range and above are therefore likely to occur. Using an optical trap with force feedback control, we studied the effect of sub- and superstall forces in both forward and backward direction on myosin-V stepping kinetics.

MATERIALS AND METHODS

Protein preparation

Chick brain myosin-V was purified essentially as described in Cheney (1998), with a Mono-Q column (Amersham Biosciences, Freiburg, Germany) for the ion exchange chromatography step. F-actin was prepared by standard methods (MacLean-Fletcher and Pollard, 1980; Pardee and Spudich, 1982), stabilized, and labeled with tetramethylrhodamine-phalloidin (Sigma-Aldrich Chemie, Taufkirchen, Germany).

Bead preparation

Polystyrene beads (1 μ l; diameter: 356 nm, 2.5% solid; Polysciences, Epelheim, Germany) were incubated in 99 μ l of buffer (25 mM imidazole-HCl, pH 7.4; 25 mM KCl; 1 mM EGTA; 10 mM DTT; 4 mM MgCl₂) containing 10 μ g/ml bovine serum albumin to preblock the surface. After 3 min of incubation, 30 pM myosin-V was added. At this motor concentration, only one out of three beads moved. This ensured that >80% of the beads that moved were driven by a single motor molecule (Block et al., 1990; Rief et al., 2000). Motility buffers (Mehta et al., 1998) (20°C–23°C) included 25 mM imidazole-HCl, pH 7.4; 25 mM KCl; 4 mM MgCl₂; 1 mM EGTA; 10 mM DTT; 2 mM ATP; and an oxygen-scavenging system to retard

Submitted September 27, 2004, and accepted for publication March 3, 2005.

Address reprint requests to Matthias Rief, E-mail: mrief@ph.tum.de.

© 2005 by the Biophysical Society

0006-3495/05/06/4402/09 \$2.00

doi: 10.1529/biophysj.104.053504

photobleaching (6 $\mu\text{g/ml}$ glucose oxidase, 1 $\mu\text{g/ml}$ catalase, and 1% glucose).

Optical tweezers experiments

Beads with motors were optically trapped and positioned over fluorescently labeled actin filaments attached to a coverslip via NEM-myosin-II (Veigel et al., 1998). The optical tweezers were similar to the instrument described in Finer et al. (1994) using an Nd:YAG Laser (1064nm; Spectra Physics, Darmstadt, Germany) and a custom built inverted microscope with a high numerical aperture objective (NA = 1.45; Olympus Deutschland, Hamburg, Germany). The position of the trapped beads was monitored using bright-field imaging onto a quadrant photodiode (SPOT4D; UDT Sensors, Hawthorne, CA). The sample was mounted on a piezo table (P-517.3CL; Physik Instrumente, Karlsruhe, Germany) controlled by a feedback loop via a digital signal processor board (M62; Innovative Integrations, Simi Valley, CA). This feedback loop with a response time of ~ 10 ms maintained a constant separation between the bead and the center of the tweezers, resulting in a constant force on the motor protein (Lang et al., 2002). Data were acquired through an analog-digital converter (MIO-16XE-50; National Instruments, Munich, Germany) with a sampling rate of 1 kHz. Actin filaments were simultaneously visualized by total internal reflection fluorescence microscopy using a frequency doubled Nd:YAG Laser (532 nm; Coherent Deutschland, Dieburg, Germany) and a CCD camera (Gen IV, Pentamax; Roper Scientific, Munich, Germany). During a run, the trap stayed at a fixed position and the sample with aligned actin filaments was moved by the piezo table following the steps of the motor (Fig. 1). Using this long-range feedback, full runs of myosin-V up to several micrometers in length could be observed without stall. The trap stiffness was calibrated for each trapped bead separately from the amplitude of the thermal diffusion (Svoboda and Block, 1994), typical trap stiffness values being 0.02–0.07 pN/nm. For some beads, calibration was cross-checked by the 3-dB corner frequency in the diffusion power spectrum. The typical corner frequency for a free trapped bead with a diameter of 350 nm was between 1 and 2 kHz. Binding of motors to the actin filament generally reduces the noise level in the position signal of a trapped bead due to additional stiffness originating from the myosin-actin cross-link. Since the stiffness of the cross-link increases further with applied tension, we saw a characteristic decrease in the noise levels of attached motors with increasing load. This was reflected in a drop of the standard deviation of the position signal of the trapped bead

from ~ 11 nm for applied loads of 0.7 pN to ~ 4 nm at 5 pN. The standard deviation of the free bead position signal at a spring constant of 0.02 pN/nm was ~ 14 nm.

Data analysis

Runs of myosin-V were visualized and analyzed with IgorPro 4.0 (WaveMetrics, Portland, OR). Step sizes and dwell times were tabulated manually by picking the dwell periods following a step. We chose the simplest kinetic model assuming that the chemomechanical cycle of the motor has two irreversible steps with different rates k_1 and k_2 :



The (normalized) dwell time distribution predicted by this model is (Rief et al., 2000):

$$P(t, k_1, k_2) = \frac{k_1 k_2}{k_1 - k_2} (\exp(-k_2 t) - \exp(-k_1 t)). \quad (2)$$

This equation is used for fitting the dwell time distributions, yielding k_1 and k_2 for different loads. Since the first data point in the dwell time distributions contains the fastest events, it may be compromised by missing these events due to limited detector response time. We therefore excluded this point from the fits. We also verified the robustness of the fitting procedure by analyzing simulated histograms. As long as the fast rate did not largely exceed the inverse of the bin width (50 s^{-1}), this method was found to be robust for histograms containing 1000 data points. To further check for possible artifacts due to the limited response time of the feedback system (~ 10 ms), we simulated runs for different values of k_1 and k_2 and analyzed the dwell time distributions. We modeled the detection probability of our detector as a function of dwell time by an error function with a rise time (detection probability = 0.5) of 20 ms. We found that for given values of $k_1 < 50 \text{ s}^{-1}$ and $k_2 < 20 \text{ s}^{-1}$, fits to the full as well as to the cut distributions reproduced the values faithfully. However, for simulated kinetics with $k_1 > 50 \text{ s}^{-1}$, the fit returned values of $\sim 50 \text{ s}^{-1}$ for the cut distributions, indicating that we could not resolve higher values due to our limited feedback response time.

Run lengths were tabulated manually. In our analysis, a run is defined as the distance the motor runs once a preset force is achieved until it detaches from the actin filament and is pulled back by the trap. In several records, the

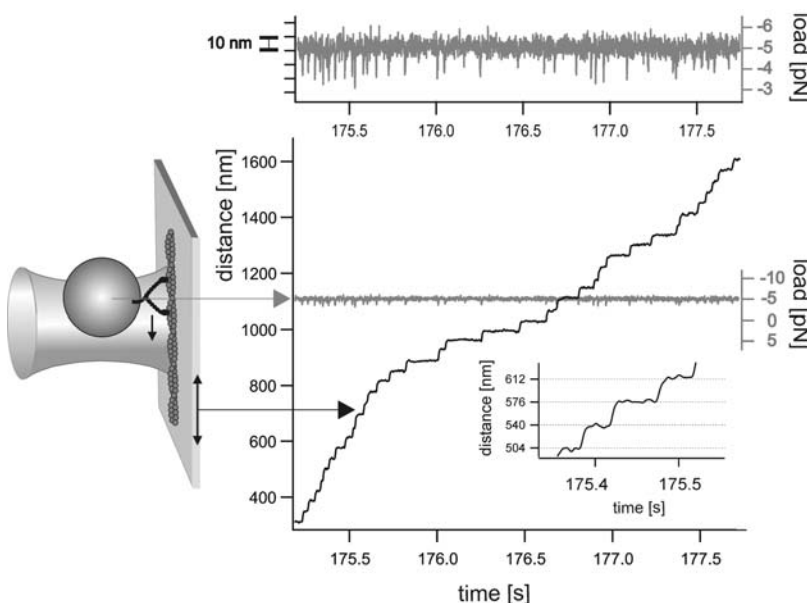


FIGURE 1 Experimental scheme of the long-range force feedback enhanced optical tweezers. The position of the trap is fixed. A feedback loop via a piezo table under the sample keeps the distance between the trap center and the position of the bead (*shaded curve*) constant as the myosin-V molecule steps along the actin filament. The position signal (*shaded curve*) is directly proportional to the force signal via the trap stiffness of 0.07 pN/nm. The piezo table follows the steps of the motor (*black curve*).

motor reattached to the filament before reaching the limit of the feedback range and started running from another point of the actin filament. If the motor was pulled back by more than ~ 2 step sizes, the event was considered a new run.

RESULTS

Systematic investigation of force-dependent stepping kinetics of molecular motors is greatly facilitated by experimental conditions where the force is kept constant (Rief et al., 2000; Visscher et al., 1999). For this purpose, we used single beam optical tweezers with feedback control over a piezo stage (see Materials and Methods for details). The beads with the motors were trapped and positioned over fluorescently labeled surface-anchored actin filaments (Fig. 1). As soon as the motor started to move along the actin filament, a feedback control was engaged, keeping the force on the motor constant. Feedback was realized via a piezo translation stage that compensated bead advances by adjusting the position of the surface-anchored actin filament similar to a treadmill (Lang et al., 2002). In combination with bright-field detection of the bead position, this setup allowed observation of continuous runs of single motors up to several micrometers in length in contrast to earlier realizations via acousto-optic deflectors (Rief et al., 2000).

Step size and dwell time at substall forces

We measured step sizes and dwell times of myosin-V under backward loads ranging from 0.7 to 1.5 pN (Fig. 2). Step sizes are distributed between 20 and 50 nm centered around

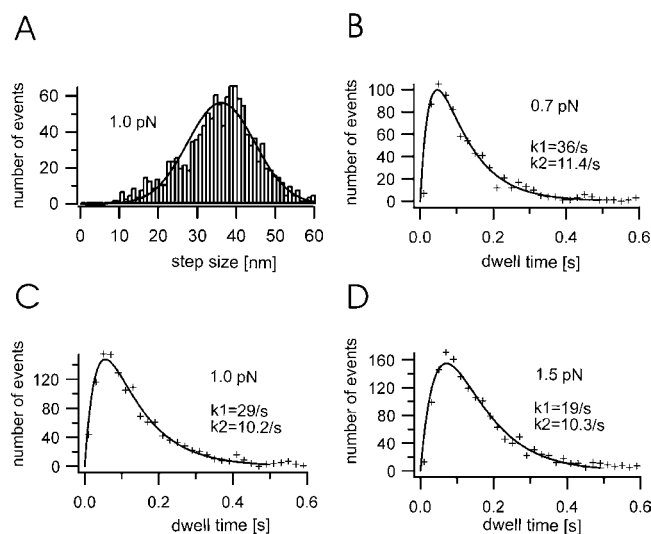


FIGURE 2 (A) An example of a typical step size distribution, fitted with a Gaussian curve. The mean step size is (36.2 ± 1) nm. (B–D) Dwell time distributions at different substall backward loads, fitted by a double exponential curve (Eq. 2). The values for the two rates are indicated in each graph separately. The first data point could be compromised by missing short events and was therefore excluded from the fits.

36 nm (sample histogram in Fig. 2 A). Although dwell time distributions are nearly single exponential, they do exhibit a peak due to the sharp decrease toward short dwell times, which indicates that more than one process is rate limiting in the chemomechanical cycle of myosin-V (Fig. 2, B–D). The simplest kinetic scheme consistent with these dwell time distributions involves two sequential irreversible steps (Eqs. 1 and 2). As shown in earlier work (Rief et al., 2000), the slower of the two rates k_2 can be identified as ADP-release. We find that both rates k_1 and k_2 are force-dependent.

At forces above ~ 1.7 pN, we could not observe continuous forward motion of the motor under constant load conditions. This value lies below values of stall forces under variable load conditions published earlier (Mehta et al., 1999; Uemura et al., 2004).

Step size and dwell time at superstall forces

To investigate the behavior of myosin-V under superstall forces in both backward and forward direction, we had to adapt our experimental procedure since a molecular motor will never step to superstall forces by itself. With a period of 3 s, we switched the feedback setpoint between 5 pN forward and 5 pN backward loads (Fig. 3). In the following, we will denote forces in forward direction by negative numbers. With no motor attached to the actin filament, the feedback tried to reach the setpoint force, and the stage rapidly moved to the respective limits of the feedback range (± 1500 nm, Fig. 3 A). If a motor attached to the actin filament while the piezo stage was at an intermediate position between the selected limits, the feedback could keep the force constant and followed the steps of myosin-V. Examples for stepping at 5 and -5 pN, respectively, are shown in Fig. 3 B. In the 5 pN backward load regime, the feedback trace shows backward steps of myosin-V. We observed up to six backward steps in a row.

It is important to rule out the possibility that the observed backward steps just reflect complete detachment of the motor and quick rebinding to an adjacent binding site 36 nm downstream of the actin filament. We therefore analyzed all traces where the feedback was switched from forward to backward pulling (Fig. 3 C). We generally observed two different classes of events. One class showed detachment of the motor upon backward pulling and no or one rebinding event to the filament over the whole feedback range (*far left* and *right traces* in Fig. 3 C). The other class of traces showed consecutive ~ 36 -nm backward steps upon application of the 5 pN backward force (Fig. 3 C, *middle trace*). The distribution of binding distances is shown in Fig. 3 D. The binding distance is the distance a motor is pulled back by the feedback before it rebinds to the actin filament (*arrows* in Fig. 3 C). The histogram shows a prominent peak at distances shorter than 50 nm (lowest bin), whereas higher binding distances occur much less frequently and are evenly distributed over the whole range (Fig. 3 D, *bottom*). The peak at steps up to 50 nm

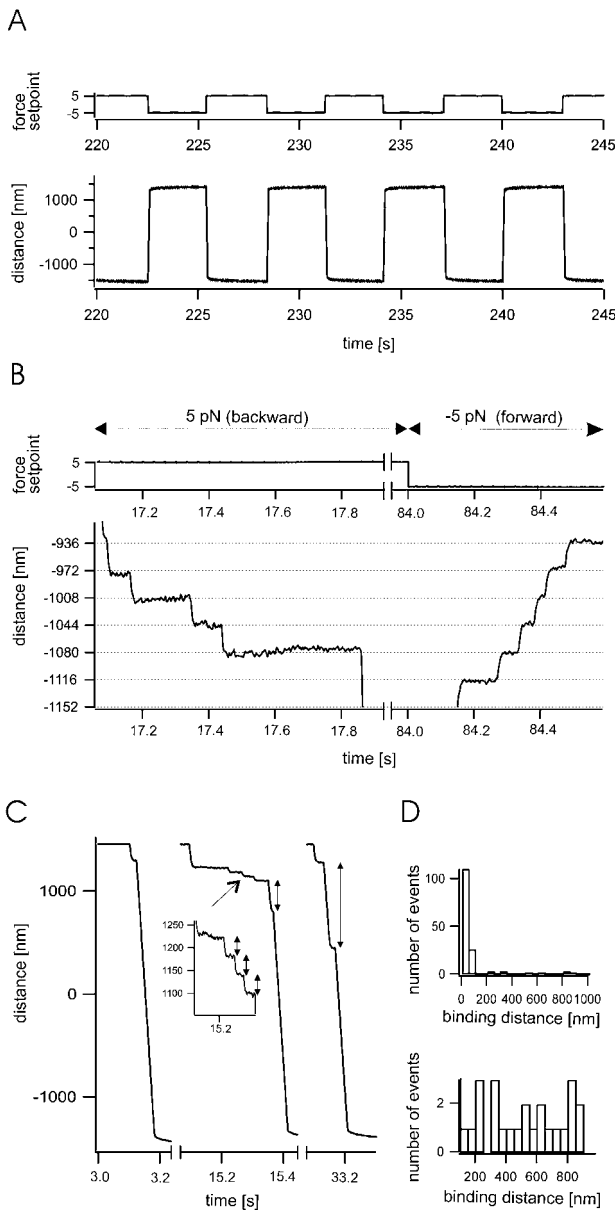


FIGURE 3 Myosin-V stepping under superstall loads. (A) In this experiment we alternatively applied forward and backward loads (-5 pN, $+5$ pN, 3 s switching time). The upper graph shows the chosen setpoint. The lower graph shows the stage position. If no motor was bound to the actin filament, the feedback followed the trigger signal and jumped between its limits. (B) Sample traces for myosin-V backward stepping at 5 pN backward load (17–18 s) and forward stepping at -5 pN forward load (>84 s). (C) Three sample traces of motor motion upon reversal of the feedback setpoint from forward to backward load. Traces show no rebinding (*left*) of the motor, several consecutive backward steps (*middle*), and a single rebinding event (*right*). Arrows mark the observed binding distance, i.e., the distance the motor is dragged by the feedback along the actin filament between detachment and reattachment. (*Inset*) Zoom into a run showing backward steps in the middle trace. (D) The distribution of binding distances shows a prominent peak at single step distances (*upper graph*), whereas longer distances are evenly distributed. The lower graph is a zoom into the upper graph excluding step values below 100 nm.

reflects backward steps, whereas the evenly distributed population at larger binding distances reflects rebinding events. The noticeable fraction of steps between 50 nm and 100 nm in the histogram presumably represents fast consecutive steps we could not resolve. To support the interpretation that the distribution in Fig. 3 *D* indeed reflects two different processes, we compared reduced χ^2 for a model for a single process (steeply decaying single exponential with zero offset) and a model for a single process plus an even distribution at high distances (single exponential with non-zero offset). The χ^2 improved from 1.6 to 0.6.

Step sizes and dwell times for 5 pN backward steps and -5 pN forward steps are summarized in Fig. 4, *A–D*. The step size distributions are again centered around 36 nm and are similar to those at lower forces. Dwell times for forward loads can be modeled by the same kinetic scheme (Eqs. 1 and 2) as for backward loads. The dwell time distribution of backward steps seems to be single exponential with a rate constant of $(7 \pm 1) \text{ s}^{-1}$ (Fig. 4 *D*).

Force dependence of kinetic rates

In Fig. 5, we summarize the force dependence of the measured rates k_1 and k_2 obtained from dwell time histograms as described above. Fig. 5 *A* shows the faster rate, k_1 , and Fig. 5 *B* describes the force dependence of the slower rate, k_2 . Forces couple to chemical rates according to Bell (1978):

$$k_i(F) = k_{0i} \exp(-Fd_i/k_B T), \quad (3)$$

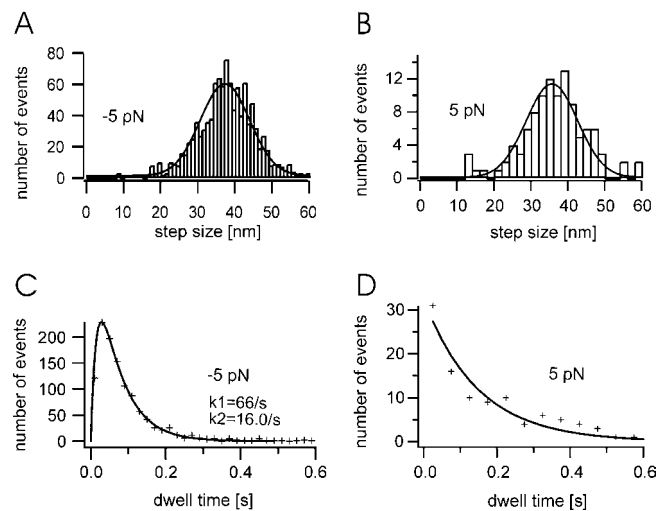


FIGURE 4 Step size and dwell time distributions at superstall forces. (A and B) The step size distributions for 5 pN backward and forward forces fitted by a Gaussian curve with the mean step size of $(35.7 \pm 1) \text{ nm}$ and $(37.3 \pm 1) \text{ nm}$, respectively. (C) The dwell time distribution at -5 pN fitted by a double exponential function (Eq. 2). (D) The dwell time distribution at 5 pN fitted by a single exponential (rate constant $(7 \pm 1) \text{ s}^{-1}$).

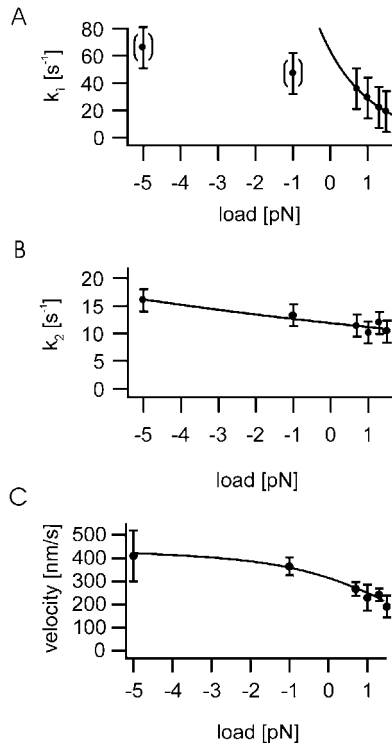


FIGURE 5 (A) Force dependence of the kinetic rate k_1 . The solid line is the fit (Eq. 3) with fitting parameters $k_{01} = (60 \pm 30) \text{ s}^{-1}$, $d_1 = (3 \pm 2) \text{ nm}$. (B) Force dependence of the kinetic rate k_2 . The solid line is the fit (Eq. 3) with fitting parameters $k_{02} = (12 \pm 2) \text{ s}^{-1}$, and $d_2 = (0.3 \pm 0.2) \text{ nm}$. (C) Force dependence of the average velocity v . The solid line is the fit (Eq. 4) to the velocity in the two rate model with fitting parameters $k_{01} = 41 \text{ s}^{-1}$, $d_1 = 3.2 \text{ nm}$, $k_{02} = 11.1 \text{ s}^{-1}$, and $d_2 = 0.05 \text{ nm}$.

where k_{0i} is the transition rate at zero load, d_i is the distance from the ground state to the transition state for the respective transition in the motor energy landscape, k_B is the Boltzmann constant, and T is the absolute temperature. The slower rate k_2 follows Eq. 3 with $d_2 = (0.3 \pm 0.2) \text{ nm}$ and $k_{02} = (12 \pm 2) \text{ s}^{-1}$ for both backward and forward loads. For backward loads, the faster rate k_1 can be described by $d_1 = (3 \pm 2) \text{ nm}$ and $k_{01} = (60 \pm 30) \text{ s}^{-1}$. However, toward forward loads, values are compromised by the detection threshold of our instrument (see Materials and Methods). We therefore put these values in brackets (Fig. 5 A) and did not include them into further analysis of the force dependence of k_1 .

It is important to note that when using a constant force feedback scheme the motor only feels a constant force on timescales longer than the feedback response time (10 ms). On shorter timescales, especially during the process of stepping, the motor feels a changing force. This can be seen in the zoomed force trace in Fig. 1, where the force drops to values of -4 pN (spikes in the force trace) during each step. However, for modeling the force dependence, this deviation from isotonic conditions has a rather small influence as long as the transition state position for the force-dependent transition is small. For a value of $d_1 = 3 \text{ nm}$ and a spring constant of

0.07 pN/nm , which was used in our experiments (see Materials and Methods), the force error does not exceed 0.2 pN .

To check the statistical relevance of the obtained results, we computed reduced χ^2 values for the fits yielding the load-dependent rates k_1 and k_2 in Fig. 5, A and B, and compared these to the respective null hypothesis that the rates do not depend on load. For rates k_1 and k_2 , the χ^2 for the null hypothesis increased by a factor of 10 as compared to the best fit.

To confirm our findings that the myosin-V cycle contains two force-dependent transitions, we also analyzed the overall velocity of the motor as a function of force. Fig. 5 C shows the force dependence of the measured average velocity v . The fit was done using a model with two force-dependent rates:

$$v = d \left(\frac{1}{k_{01} \exp(-Fd_1/k_B T)} + \frac{1}{k_{02} \exp(-Fd_2/k_B T)} \right)^{-1} \quad (4)$$

where d is the step size set to 36 nm . The obtained values for $k_{01} = 41 \text{ s}^{-1}$, $d_1 = 3.2 \text{ nm}$, and $k_{02} = 11.1 \text{ s}^{-1}$, $d_2 = 0.05 \text{ nm}$ come close to the values from the fits of the single rate values (Fig. 5, A and B).

Run length

We measured run length distributions $p(r)$ for forward movement at forces ranging from -5 to 1.5 pN (Fig. 6, A–D). All run length distributions closely follow a single exponential distribution:

$$p(r) \propto \exp(-r/c). \quad (5)$$

We find the characteristic run length for forward movement, c , is almost independent of force for all forces measured (Fig. 6 E).

Fig. 6 F shows the run length distribution for backward movement at 5 pN . It also shows a single exponential distribution but with a shorter characteristic run length of $\sim 80 \text{ nm}$.

DISCUSSION

Although a definitive picture of the chemomechanical cycle of myosin-V has not yet evolved, many aspects of myosin-V motility are consistent with the model briefly outlined in Fig. 7 (Mehta, 2001; Rief et al., 2000; Rosenfeld and Lee Sweeney, 2004; Vale, 2003; Veigel et al., 2002). During most of the cycle, myosin-V is bound with both heads to the actin filament. Starting from a conformation with both heads bound and the rear head nucleotide free, ATP will bind to the rear head and dissociate this head from the actin filament, and the leading head with ADP bound will complete its power stroke. ATP hydrolysis occurs rapidly and the now forward head binds to actin. Then both heads are in the ADP bound state and possibly intramolecular strain prevents premature ADP-release from the leading head. ADP-release

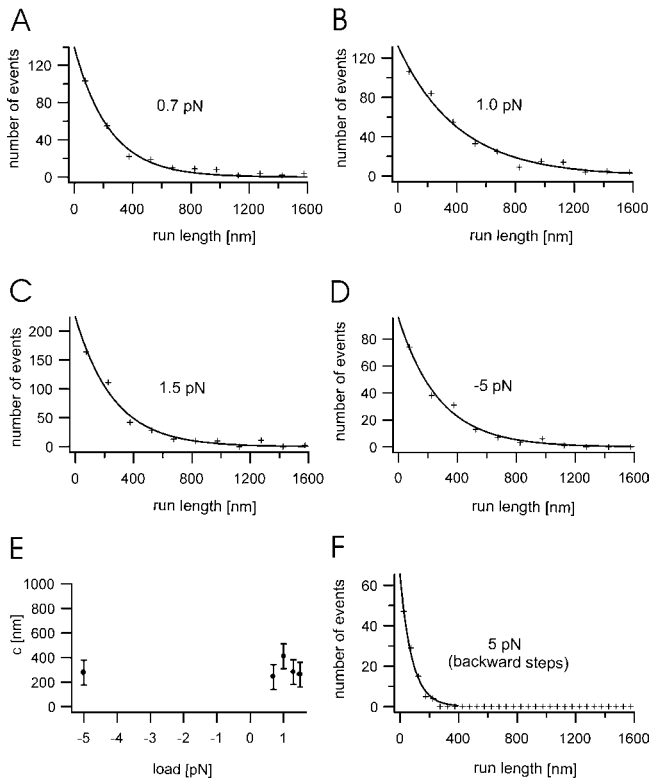


FIGURE 6 (A–D) Run length distributions of the forward movement at different loads. Positive values represent backward loads, negative values forward loads. Solid lines are single exponential fits (Eq. 5). (E) Load dependence of the characteristic run length c . (F) Run length distribution for the backward steps at 5 pN also fitted with Eq. 5.

from the rear head is the rate-limiting transition in the whole cycle occurring at $\sim 12 \text{ s}^{-1}$ (De La Cruz et al., 1999; Mehta, 2001; Rief et al., 2000; Rosenfeld and Lee Sweeney, 2004; Vale, 2003; Veigel et al., 2002).

Step size

Step size distributions in a wide range of loads between -5 and 1.5 pN are virtually independent of force, centered around 36 nm . The broad distribution reflects the flexibility of myosin-V when sampling the accessible binding sites during a step (Rief et al., 2000; Rock et al., 2001). On average, however, the actin pseudo helix repeat is extremely well reproduced at all forces with a variability of $< 2 \text{ nm}$. This result is consistent with recent single-molecule fluorescence polarization measurements by Forkey et al. (2003) where the authors report broad distributions of axial angles relative to the actin filament. It is important to point out the difference in our experimental geometry using surface bound actin filaments as compared to the study of Ali et al. (2002) who observe rotation of a single myosin motor around a suspended actin filament. These authors find an average step size of 34.8 nm . In an assay with surface-immobilized actin filaments, myosin-V seems to be able to

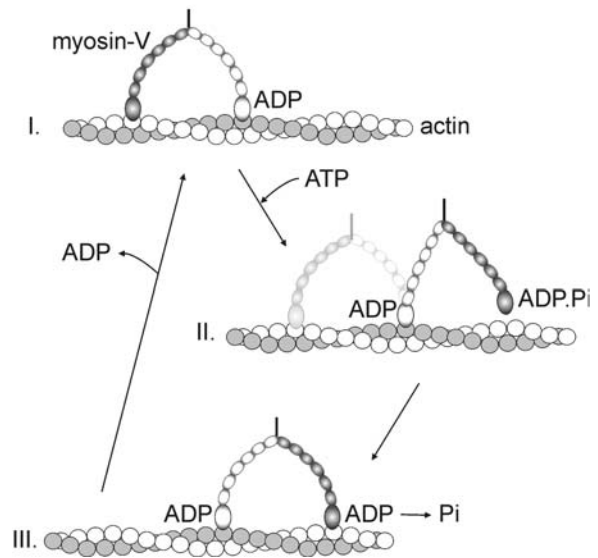


FIGURE 7 Model of the chemomechanical cycle of myosin-V. The two lever arms with the heads of the myosin-V molecule are depicted as white and shaded ellipses to distinguish them. The cycle begins with both heads bound to actin, the rear head is nucleotide free, and the forward head contains ADP (I). ATP binds to the rear head, dissociates this head from the actin filament, and the leading head completes its power stroke (II). ATP hydrolysis occurs rapidly, and the now forward head binds to actin. After phosphate release, both heads are in the ADP bound state and possibly intramolecular strain prevents premature ADP-release from the leading head (III). The rate-limiting step of ADP-release from the rear head completes the cycle.

adjust its step size so that long linear runs along the filament are possible.

The slightly increased number of measured step sizes between 10 and 20 nm in Fig. 2 A may reflect an additional population of substeps as recently reported (Uemura et al., 2004). However, we do not consistently observe that subsequent substeps add up to a full step.

Force-dependent transitions in the chemomechanical cycle

At backward loads between 0.7 and 1.5 pN , we find two force-dependent rates. The slower rate, k_2 , previously identified as ADP release (Rief et al., 2000), depends only weakly on force with a transition state position (Eq. 3) of $d_2 = (0.3 \pm 0.2) \text{ nm}$ (Fig. 5 B), whereas the faster rate, k_1 , exhibits a stronger force dependence with $d_1 = (3 \pm 2) \text{ nm}$ (Fig. 5 A). Supporting this, similar values for the force dependence of k_1 and k_2 also fit the overall average velocity (Fig. 5 C). We conclude that in a double headed myosin-V, ADP-release is only weakly force dependent. Even at forward forces of up to -5 pN , the motor runs faster by only a factor of ~ 1.5 . At first sight this result appears at odds with studies of single headed myosin-V constructs showing a 5-nm portion of the motor power stroke coupled to ADP release (Veigel et al., 2002). A strong sensitivity of this

transition on force would therefore be expected, assuming the transition state position d is placed somewhere in the middle of this transition. Moreover, single-molecule measurements with smooth muscle myosin (Veigel et al., 2003) have shown a much stronger force dependence of ADP release ($d = 1.3$ nm) on single smooth muscle myosin cross-bridges. Recently Vilfan (2005) is suggesting that internal conformational transitions within a two-headed motor with both heads firmly attached to the actin filament will hardly affect the center of mass position of this motor. He calculated that a conformational change on the order of 5 nm within a single-headed construct will lead to only a movement of the center of mass of a double headed motor well below 0.2 nm. The conformational change will be mostly absorbed by the bending of the lever arms. This argument explains our observation that ADP-release in a double headed motor can be largely insensitive to external forces (Fig. 5 B), whereas in the single headed motor ADP-release may strongly depend on force. Our results are therefore still in agreement with the widely believed mechanism of internal strain coordinating the two heads by slowing down ADP-release in the head experiencing backward strain and accelerating ADP-release in the head pulled forward (Fig. 7 III) (Rief et al., 2000; Rosenfeld and Lee Sweeney, 2004; Veigel et al., 2002). This result offers an intriguing insight into how nature can design a double headed motor mechanically robust against external forces by coupling two heads, each of them being force sensitive. This robustness is especially important considering that tug-of-war scenarios between myosin-V and, e.g., kinesins are likely to occur *in vivo*. Interestingly, Altman et al. (2004) have recently reported a small load dependence of ADP-release at saturating ATP conditions also for myosin-VI.

Analyzing the distributions of dwell times under constant load allows direct observation of the load dependence of ADP-release. Recently, Uemura et al. (2004) have interpreted a strongly load-dependent rate with a transition state position, $d \sim 12$ nm as ADP-release. As a consequence of such a strong load dependence, ADP-release under zero load would have to occur at a rate of ~ 1000 s⁻¹. This is hard to reconcile with a value of ~ 12 s⁻¹ measured in various assays (De La Cruz et al., 1999; Mehta, 2001; Rief et al., 2000; Rosenfeld and Lee Sweeney, 2004; Vale, 2003; Veigel et al., 2002). On the other hand, an additional load-dependent rate with such a large d could explain the sharp drop of velocity close to stall also in our data.

In contrast to ADP-release, we find that the faster of the two rates, k_1 , shows a stronger force dependence in the backward force regime with $d_1 = (3 \pm 2)$ nm (Fig. 5 A). It is important to note that the two-rate model (Eq. 1) we use to analyze our distributions is the simplest approximation, and k_1 is merely a compound rate reflecting the sum of all faster transitions within the chemomechanical cycle of the motor. As k_1 exhibits a pronounced force dependence in the backward load regime with a large transition state position,

considerable movement along the actin filament must be associated with it. Since all conformational transitions in a state with both heads bound will not lead to a considerable center of mass motion (Vilfan, 2005), this transition probably occurs in a conformation with only one head bound. We can therefore rule out the 5-nm portion of the power stroke associated with ADP-release as a candidate. Only two possible candidates for k_1 thus remain: the main power stroke or the diffusional search of the leading head searching for its correct binding site. Since part of the diffusional search will be absorbed by building up internal strain, this process will only lead to a center of mass motion of ~ 5 nm (Veigel et al., 2002). We favor the latter model for two reasons: First, a diffusive search is likely to have a transition state very close to the completion of its motion, and a value for $d_1 = (3 \pm 2)$ nm comes close to the expected 5 nm. Second, if the transition state for the main power stroke were positioned so closely to the starting conformation, the kinetics for the power stroke would still be ~ 20 s⁻¹ at stall force conditions of 1.7 pN (Eq. 3), and we would expect stall to be characterized by rapid oscillations between pre- and post power stroke conformations, which we do not observe.

Backward steps

At superstall forces of 5 pN, the motor can no longer step forward but rather performs backward steps. There are several possibilities how backward stepping of molecular motors can be coupled to the kinetic cycle. In the case of kinesin, for example, backward stepping could be correlated with ATP hydrolysis (Nishiyama et al., 2002). As recently demonstrated for the rotary motor F₁-ATPase, forced backward motion in a tightly coupled scheme results in ATP synthesis (Itoh et al., 2004). Although this mechanism may be applicable to a linear motor like myosin-V, the concentrations of ADP and Pi in our assays were far too low to allow tightly coupled backward stepping at the high rates (7 s⁻¹) we observed in our experiment. We therefore favor a less tightly coupled model of force-induced myosin-V backward stepping. We assume that at superstall forces, the high loads induce unbinding of the leading head. Force reverses the power stroke in the now fully loaded trailing head. The other head can then bind at the new trail position. Investigations of the coordination of the two heads during forced backward motion and the influence of ATP, ADP, and phosphate concentrations require further experiments.

Run length

A characteristic property of processive motors is the distance they are able to walk before detaching from a filament. In our laser trap experiments, we find relatively short characteristic run lengths for myosin-V of only ~ 10 steps. This number appears small compared to results from single-molecule fluorescence measurements or *in vitro* gliding assays (Baker

et al., 2004; Mehta et al., 1999; Sakamoto et al., 2003). However, in our experiments the feedback pulls the motor off the track as soon as it detaches (see also Materials and Methods). It therefore directs diffusion of the motor away from its track and likely prevents rebinding to the same position on the track as compared to other assays.

As for kinesin (Block et al., 1990; Schnitzer et al., 2000; Vale et al., 1996), we find run lengths for given loads single exponentially distributed (Fig. 6, A–E), indicating that a single process induces detachment. In contrast to kinesin, where run lengths depend exponentially on load, the myosin-V run length is essentially load independent. Force independence of run length therefore indicates that the bond, which ruptures upon detachment, exhibits a transition state position very close to the unloaded conformation. A candidate for such a short range potential would be the myosin-actin bond. Presumably, as suggested in Baker et al. (2004) and Sakamoto et al. (2003), the run is most likely at risk of being terminated when only one head is bound to actin (Fig. 7 II).

CONCLUSION

Most of the time molecular motors when moving cargo freely through an aqueous solution will only experience mechanical load in the femtonewton range. However, inside a cell when moving through a dense cytoskeletal meshwork and possibly fighting against colocalized stronger motors, the response of myosin-V against external load may be crucial for its performance. In our study, myosin-V proved amazingly robust against external forces. Even high loads did not affect its run length and velocity considerably. By combining two heads to a double headed motor, nature has produced a molecular motor which is much more robust against external force than the individual components it consists of.

We thank C. Antrecht, H. Kirpal, M. Rusp, and K. Voigt for assistance in the purification of myosin-V and actin and J. C. M. Gebhardt, A. Vilfan, and M. Reisinger for helpful discussions.

This work was supported by an SFB 486 grant of the Deutsche Forschungsgemeinschaft; M. Vilfan acknowledges support from the European Union through a Marie Curie Fellowship grant (No. HPMF-CT-2002-01887).

REFERENCES

Ali, M. Y., S. Uemura, K. Adachi, H. Itoh, K. Kinoshita Jr., and S. Ishiwata. 2002. Myosin V is a left-handed spiral motor on the right-handed actin helix. *Nat. Struct. Biol.* 9:464–467.

Altman, D., H. L. Sweeney, and J. A. Spudich. 2004. The mechanism of myosin VI translocation and its load-induced anchoring. *Cell*. 116:737–749.

Baker, J. E., E. B. Kremntsova, G. G. Kennedy, A. Armstrong, K. M. Trybus, and D. M. Warshaw. 2004. Myosin V processivity: multiple

kinetic pathways for head-to-head coordination. *Proc. Natl. Acad. Sci. USA*. 101:5542–5546.

Bell, G. I. 1978. Models for the specific adhesion of cells to cells. *Science*. 200:618–627.

Block, S. M., L. S. Goldstein, and B. J. Schnapp. 1990. Bead movement by single kinesin molecules studied with optical tweezers. *Nature*. 348:348–352.

Cheney, R. E. 1998. Purification and assay of myosin V. *Methods Enzymol.* 298:3–18.

De La Cruz, E. M., A. L. Wells, S. S. Rosenfeld, E. M. Ostap, and H. L. Sweeney. 1999. The kinetic mechanism of myosin V. *Proc. Natl. Acad. Sci. USA*. 96:13726–13731.

Finer, J. T., R. M. Simmons, and J. A. Spudich. 1994. Single myosin molecule mechanics: piconewton forces and nanometre steps. *Nature*. 368:113–119.

Forkey, J. N., M. E. Quinlan, M. A. Shaw, J. E. Corrie, and Y. E. Goldman. 2003. Three-dimensional structural dynamics of myosin V by single-molecule fluorescence polarization. *Nature*. 422:399–404.

Huang, J. D., S. T. Brady, B. W. Richards, D. Stenolen, J. H. Resau, N. G. Copeland, and N. A. Jenkins. 1999. Direct interaction of microtubule- and actin-based transport motors. *Nature*. 397:267–270.

Itoh, H., A. Takahashi, K. Adachi, H. Noji, R. Yasuda, M. Yoshida, and K. Kinoshita. 2004. Mechanically driven ATP synthesis by F1-ATPase. *Nature*. 427:465–468.

Lang, M. J., C. L. Asbury, J. W. Shaevitz, and S. M. Block. 2002. An automated two-dimensional optical force clamp for single molecule studies. *Biophys. J.* 83:491–501.

MacLean-Fletcher, S., and T. D. Pollard. 1980. Identification of a factor in conventional muscle actin preparations which inhibits actin filament self-association. *Biochem. Biophys. Res. Commun.* 96:18–27.

Mehta, A. 2001. Myosin learns to walk. *J. Cell Sci.* 114:1981–1998.

Mehta, A. D., J. T. Finer, and J. A. Spudich. 1998. Use of optical traps in single-molecule study of nonprocessive biological motors. *Methods Enzymol.* 298:436–459.

Mehta, A. D., R. S. Rock, M. Rief, J. A. Spudich, M. S. Mooseker, and R. E. Cheney. 1999. Myosin-V is a processive actin-based motor. *Nature*. 400:590–593.

Mermall, V., P. L. Post, and M. S. Mooseker. 1998. Unconventional myosins in cell movement, membrane traffic, and signal transduction. *Science*. 279:527–533.

Nishiyama, M., H. Higuchi, and T. Yanagida. 2002. Chemomechanical coupling of the forward and backward steps of single kinesin molecules. *Nat. Cell Biol.* 4:790–797.

Pardee, J. D., and J. A. Spudich. 1982. Purification of muscle actin. *Methods Cell Biol.* 24:271–289.

Purcell, T. J., C. Morris, J. A. Spudich, and H. L. Sweeney. 2002. Role of the lever arm in the processive stepping of myosin V. *Proc. Natl. Acad. Sci. USA*. 99:14159–14164.

Reck-Peterson, S. L., D. W. Provan Jr., M. S. Mooseker, and J. A. Mercer. 2000. Class V myosins. *Biochim. Biophys. Acta*. 1496:36–51.

Rief, M., R. S. Rock, A. D. Mehta, M. S. Mooseker, R. E. Cheney, and J. A. Spudich. 2000. Myosin-V stepping kinetics: a molecular model for processivity. *Proc. Natl. Acad. Sci. USA*. 97:9482–9486.

Rock, R. S., S. E. Rice, A. L. Wells, T. J. Purcell, J. A. Spudich, and H. L. Sweeney. 2001. Myosin VI is a processive motor with a large step size. *Proc. Natl. Acad. Sci. USA*. 98:13655–13659.

Rosenfeld, S. S., and H. Lee Sweeney. 2004. A model of Myosin V processivity. *J. Biol. Chem.* 279:40100–40111.

Sakamoto, T., F. Wang, S. Schmitz, Y. Xu, Q. Xu, J. E. Molloy, C. Veigel, and J. R. Sellers. 2003. Neck length and processivity of myosin V. *J. Biol. Chem.* 278:29201–29207.

Schnitzer, M. J., K. Visscher, and S. M. Block. 2000. Force production by single kinesin motors. *Nat. Cell Biol.* 2:718–723.

Svoboda, K., and S. M. Block. 1994. Biological applications of optical forces. *Annu. Rev. Biophys. Biomol. Struct.* 23:247–285.

- Uemura, S., H. Higuchi, A. O. Olivares, E. M. De La Cruz, and S. Ishiwata. 2004. Mechanochemical coupling of two substeps in a single myosin V motor. *Nat Struct Mol Biol.* 11:877–883.
- Vale, R. D. 2003. Myosin V motor proteins: marching stepwise towards a mechanism. *J. Cell Biol.* 163:445–450.
- Vale, R. D., T. Funatsu, D. W. Pierce, L. Romberg, Y. Harada, and T. Yanagida. 1996. Direct observation of single kinesin molecules moving along microtubules. *Nature.* 380:451–453.
- Veigel, C., M. L. Bartoo, D. C. White, J. C. Sparrow, and J. E. Molloy. 1998. The stiffness of rabbit skeletal actomyosin cross-bridges determined with an optical tweezers transducer. *Biophys. J.* 75:1424–1438.
- Veigel, C., J. E. Molloy, S. Schmitz, and J. Kendrick-Jones. 2003. Load-dependent kinetics of force production by smooth muscle myosin measured with optical tweezers. *Nat. Cell Biol.* 5:980–986.
- Veigel, C., F. Wang, M. L. Bartoo, J. R. Sellers, and J. E. Molloy. 2002. The gated gait of the processive molecular motor, myosin V. *Nat. Cell Biol.* 4:59–65.
- Vilfan, A. 2005. Elastic lever-arm model for myosin V. *Biophys. J.* 88:3792–3805.
- Visscher, K., M. J. Schnitzer, and S. M. Block. 1999. Single kinesin molecules studied with a molecular force clamp. *Nature.* 400:184–189.
- Wang, F., L. Chen, O. Arcucci, E. V. Harvey, B. Bowers, Y. Xu, J. A. Hammer 3rd, and J. R. Sellers. 2000. Effect of ADP and ionic strength on the kinetic and motile properties of recombinant mouse myosin V. *J. Biol. Chem.* 275:4329–4335.
- Yildiz, A., J. N. Forkey, S. A. McKinney, T. Ha, Y. E. Goldman, and P. R. Selvin. 2003. Myosin V walks hand-over-hand: single fluorophore imaging with 1.5-nm localization. *Science.* 300:2061–2065.